Microchemical imaging of iodine distribution in the brown alga Laminaria digitata suggests a new mechanism for its accumulation. J Biol Inorg Chem

ARTICLE *in* JBIC JOURNAL OF BIOLOGICAL INORGANIC CHEMISTRY · MARCH 2008

Impact Factor: 2.54 · DOI: 10.1007/s00775-007-0319-6 · Source: PubMed

J Biol Inorg Chem (2008) 13:257–269
DOI 10.1007/s00775-007-0319-6

ORIGINAL PAPER

Microchemical imaging of iodine distribution in the brown alga *Laminaria digitata* suggests a new mechanism for its accumulation

Elodie Françoise Verhaeghe · Aurélien Fraysse · Jean-Luc Guerquin-Kern · Ting-Di Wu · Guillaume Devès · Charles Mioskowski · Catherine Leblanc · Richard Ortega · Yves Ambroise · Philippe Potin

Received: 11 July 2007 / Accepted: 1 November 2007 / Published online: 16 November 2007

Abstract Brown algal kelp species are the most efficient iodine accumulators among all living systems, with an average content of 1.0% of dry weight in *Laminaria digitata*. The iodine distributions in stipe and blade sections from *L. digitata* were investigated at tissue and subcellular levels. The quantitative tissue mapping of iodine and other trace elements (Cl, K, Ca, Fe, Zn, As and Br) was provided by the proton microprobe with spatial resolutions down to 2 μm. Chemical imaging at a subcellular resolution (below 100 nm) was performed using the secondary ion mass spectrometry microprobe. Sets of samples were prepared by both chemical fixation and cryofixation procedures. The latter prevented the diffusion and the leaching of labile inorganic iodine species, which were estimated at around 95% of the total content by neutron activation analysis. The distribution of iodine clearly shows a huge, decreasing gradient from the meristoderm to the medulla. The contents of iodine reach very high levels in the more external cell layers, up to 191 ± 5 mg g^{-1} of dry weight in stipe sections. The peripheral tissue is consequently the main storage compartment of iodine. At the subcellular level, iodine is mainly stored in the apoplasm and not in an intracellular compartment as previously proposed. This unexpected distribution may provide an abundant and accessible source of labile iodine species which can be easily remobilized for potential chemical defense and antioxidative activities. According to these imaging data, we proposed new hypotheses for the mechanism of iodine storage in *L. digitata* tissues.

Keywords Iodine · *Laminaria digitata* · Tissue distribution · Subcellular distribution · Proton microprobe · Secondary ion mass spectrometry microprobe

Abbreviations
LOD Limit of detection
NAA Neutron activation analysis

In memory of Dr. Charles Mioskowski, "Miko," who died on 2 June 2007.

E. F. Verhaeghe (✉) · C. Mioskowski · Y. Ambroise
iBiTec-S, Service de Chimie Bioorganique et de Marquage,
CEA Saclay, Bât. 547,
91191 Gif-sur-Yvette Cedex, France
e-mail: elodie.verhaeghe@cea.fr

Y. Ambroise
e-mail: yves.ambroise@cea.fr

C. Leblanc · P. Potin (✉)
UMR7139, Marine Plants and Biomolecules,
Laboratoire International Associé,
Dispersal and Adaptation in Marine Species,
Station Biologique,
Université Pierre et Marie Curie-Paris 6/CNRS,
29682 Roscoff Cedex, France
e-mail: potin@sb-roscoff.fr

A. Fraysse · G. Devès · R. Ortega
CNRS/Université Bordeaux 1,
Groupe d'Imagerie Chimique Cellulaire et Spéciation,
CNAB UMR 5084,
BP 120 Le Haut-Vigneau,
33175 Gradignan Cedex, France
e-mail: ortega@cenbg.in2p3.fr

J.-L. Guerquin-Kern · T.-D. Wu
Laboratoire de Microscopie Ionique,
Institut Curie,
91405 Orsay, France
e-mail: jean-luc.guerquin-kern@curie.u-psud.fr

J.-L. Guerquin-Kern · T.-D. Wu
INSERM U759,
91405 Orsay, France

PIXE	Particle-induced X-ray emission
RBS	Rutherford backscattering spectrometry
SIMS	Secondary ion mass spectrometry
vHPO	Vanadium-dependent haloperoxidase
VIOCs	Volatile iodinated organic compounds
vIPO	Vanadium-dependent iodoperoxidase
XAS	X-ray absorption spectroscopy

Introduction

Iodine is an essential micronutrient for the human diet owing to its involvement in the synthesis of thyroid hormones. Iodine deficiency leads to goiter and various disorders associated with growth and development, commonly referred to as iodine deficiency disorders, and still constitutes a global health problem [1–3]. For terrestrial life, the major iodine source is the marine environment. The biogeochemical cycle of iodine is controlled by intense exchanges in the marine boundary layer, from oceans to the atmosphere. This process involves the emission of volatile iodinated organic compounds (VIOCs) and molecular iodine (I_2) by phytoplankton and macrophytic algae. In the atmosphere, these VIOCs and I_2 are broken down by photolysis to generate new oxidized species which are eventually involved in aerosol particle formation and cloud condensation nuclei formation [4]. Iodine is subsequently deposited back on land by rain-out or by dry deposition of aerosols, which allows its availability for the human diet [5, 6].

In coastal areas, the role of brown algal kelps in the global cycle of iodine has recently been reinvestigated [4]. It is well known that kelps are the most efficient iodine accumulators among all living systems. Their iodine content reaches up to 5% of dry weight in *Laminaria digitata* species, which explains their use as an iodine source [7]. In addition, recent reports found that brown macroalgae are major contributors to the iodine flux owing to their emission of I_2, which is believed to be significantly greater than that of VIOCs [8]. This molecular iodine is suggested to have a significant impact on the chemistry of the atmosphere by catalyzing the marine boundary layer depletion of ozone and to be the main precursor of the coastal particles [8–11]. From a physiological point of view, VIOCs and I_2 are likely to be generated by vanadium-dependent haloperoxidases (vHPOs) and to be involved in potential chemical defense and antioxidant activities in kelps [12, 13].

The understanding of iodine uptake and release by kelps consequently has environmental [14], radioecological and health interest. However, although the high iodine content in kelps has been reported since the nineteenth century, the biochemical pathways of iodine accumulation and its physiological significance have still not been fully elucidated.

From a macroscopic point of view, iodine is not homogeneously distributed in kelp sporophytes. The iodine content increases from the meristematic area to the distal extremities of the blade and to the holdfast in *L. digitata* [7]. The blades and the stipes of Laminariales consist of three different tissues: the meristoderm, the cortex and the medulla. The meristoderm is similar to higher-plant epidermis, but it is photosynthetic. It is composed of small cells with high plastid content and is covered with a layer of mucilage. A thick layer of cortex lies between the meristoderm and the center of the stipe or the blade, which is composed of elongated cells (called hyphae), and refers to the medulla [15]. In stipe sections of *L. hyperborea*, an old report showed that iodine accumulates more in the peripheral tissue—meristoderm and outer cortex—than in the inner tissues [16]. Up to now, no accurate tissue quantifications of iodine have been reported in the literature.

In Laminariales, several speciation studies have concluded that iodine is mainly stored in a labile inorganic form (up to 90%) analyzed to be iodide. The remainder consists of iodinated amino acid residues, especially iodotyrosine [17–20]. All these speciation studies remain questionable since they rely on extracting iodine species from frozen or dehydrated seaweed samples. During the extraction process, the modification of the redox potential induced by osmotic shock, the dilution and the nonphysiological pH of aqueous buffers probably altered the iodine speciation in kelps [21]. Consequently, one cannot assert that iodine is stored as iodide in Laminariales tissues. Nevertheless, inorganic iodine species must be the main storage forms in Laminariales since these same studies gave very different iodine speciation profiles for algal species which do not belong to this order [19, 22].

Concerning the mechanism of iodine uptake by kelps, Küpper et al. [23] confirmed the conjectures of Kylin [24] and Shaw [25] by underlining the involvement of vHPOs. Küpper et al. [23] proposed that, using H_2O_2 as a cosubstrate, apoplastic vHPOs facilitate the iodine uptake by catalyzing the conversion of I^- to a more lipophilic species—IOH or I_2—which easily diffuses across cell membranes. In order to preserve the favorable electrochemical potential gradient, the oxidized species is then reduced back to iodide in the intracellular compartment and stored in the cytosol or in organelles such as vacuoles (Fig. 6a). This mechanism was recently strengthened by the identification of vanadium-dependent iodoperoxidases (vIPOs) in *L. digitata* which selectively oxidize iodide [26, 27]. However, Leblanc et al. [28] point out that such a mechanism of uptake is a real physiological challenge: an

efficient reducing intracellular process is required and the storage compartment membrane must be almost impermeable to I^-, in order to preserve the huge intracellular iodide concentration (estimated to be around 30 mM). An alternative mechanism can be deduced from Klotz and Benz's study [29]. They showed that the transport of I^- and Br^- across artificial lipid bilayer membranes was mediated by oxidized species such as I_2 and Br_2. Their kinetic model proposes that X_3^- acts as a shuttle which liberates X^- at the other side of the membrane [29]. Such a mechanism is questionable since it involves the continuous presence of reactive species such as I_2 or Br_2 inside the membranes, which appears potentially damaging for living cells.

To our knowledge, no study about the subcellular localization of iodine has been carried out to confirm these mechanisms. Before the investigations of Küpper et al., Pedersen and Roomans [30] performed X-ray microanalyses on chemically fixed sections from Laminariales stipes. Iodine and bromine were detected in cell walls and middle lamellae and, anecdotally, in polyphenol-rich vesicles (physodes). However, the authors mentioned that the chemical fixation, used for sample preparations, implied the leaching of diffusible species and concluded that only organically bound iodine, which represents less than 10% of the total iodine in Laminariales, was likely to be detected [30]. In this context, the tissue and subcellular distributions of iodine species are still key elements in elucidating the mechanism of its uptake and its physiological role in kelps.

In this paper, we describe, for the first time, the complementary use of two elemental microimaging techniques in order to elucidate the tissue and subcellular distributions in *L. digitata* sections: the proton microprobe and the secondary ion mass spectrometry (SIMS) microprobe [31, 32]. The proton microprobe, which is a multielemental and quantitative method, provided the quantitative tissue distribution of iodine and other elements (Cl, K, Ca, Fe, Zn, As and Br) in blade and stipe sections with a spatial resolution down to 2 μm. The subcellular distributions of total iodine were investigated by SIMS imaging, which displays very high sensitivity and spatial resolution (down to 100 nm). Samples were prepared by cryofixation procedures in order to prevent the diffusion and the leaching of labile iodine species, which is crucial in the case of *L. digitata* tissues. A set of samples was also prepared by a classic chemical-fixation procedure for SIMS microprobe analyses in order to compare our results with those of Pedersen and Roomans and to determine the proportion of labile iodine forms and the effect of the fixation procedure on the subcellular iodine distribution.

Our results reveal an unexpected subcellular distribution of iodine, which raises new questions and new hypotheses for the mechanism of its storage in brown algal kelps.

Materials and methods

Plant materials

L. digitata sporophytes, between 10 and 100 cm in length, were collected from the shore in the vicinity of Roscoff (Brittany, France), and maintained for a few days in running seawater tanks with an illumination of 60 μE m^{-2} s^{-1} and a photoperiod of 12 h light and 12 h dark.

Sample preparation for proton microprobe analyses

L. digitata sporophytes (80 cm in length) were rapidly washed in deionized water. Tissue samples were taken from the stipe and the meristematic area of the blade. Thick cross sections (0.3–0.5 mm) were cut using a scalpel, immediately cryofixed in liquid nitrogen chilled isopentane and freeze-dried into a cryostat at −35 °C for 5 days (adapted from the method of Ortega et al. [33]). The sections were then placed on 2 μm polycarbonate foils stretched onto drilled aluminum holders.

Sample preparation for SIMS microprobe analyses

To compare the effect of the fixation procedure on the subcellular distribution of iodine and bromine, two sets of samples were prepared.

The first set of samples was obtained by a classic procedure of chemical fixation. Thick cross sections (2 mm thick) from the blade and the stipe of several sporophytes were fixed in seawater containing 3% (v/v) glutaraldehyde and then in seawater containing 1.5% paraformaldehyde. Fixation was followed by a series of rinses in seawater/ethanol solution. The percentage of ethanol was increased by 25% in each successive step. The samples were then dehydrated in ethanol, infiltrated by Spurr's resin for 4 days and, finally, polymerized.

To prevent the redistribution of labile species, the second set of samples was prepared by a cryofixation procedure derived from animal tissue preparation previously described by Guerquin-Kern et al. [34]. Cross sections from blade and stipe (0.5–1 mm thick) were fixed by slam-freezing on a metal mirror precooled at −190 °C and dehydrated by freeze-drying, in a vacuum (0.2 Pa), starting at −110 °C and going to −10 °C. The samples were then infiltrated by Spurr's resin, with the temperature slowly increasing from −10 to 20 °C, and were subsequently polymerized at 65 °C.

For each sample, serial semithin sections (0.4 μm) were cut using an ultramicrotome and collected on water. By quickly picking up sections and laying them down on a

prewarmed silicon holder for SIMS imaging (typically in less than 10 s), one minimizes the risk of relocating diffusible elements at the upper surface of the section which is not in contact with water. A second set of semithin sections was placed on glass slides for light microscopy to control the histological aspect and to select the area of interest.

Determination of iodine and bromine content in cryofixed and chemically fixed sections by neutron activation analysis

The total iodine content of unembedded cryofixed and chemically fixed sections from blade and stipe of *L. digitata* was deduced from the analyses of pieces of the same regions of sporophytes (40 cm in length, with stipes shorter than 10 cm and blades less than 10 cm in width), which were rapidly washed in deionized water and subjected to the following treatments. The first set of samples, corresponding to thick cross sections (0.3–0.5 mm), was cut using a scalpel, immediately cryofixed in liquid nitrogen and freeze-dried. The second set of samples was obtained by a classic procedure of chemical fixation. Thick cross sections (0.3–0.5 mm) from the blade and the stipe of two sporophytes were fixed in seawater containing 3% (v/v) glutaraldehyde and then in seawater containing 1.5% paraformaldehyde. The fixation was followed by a series of rinses in seawater/ethanol solution. The percentage of ethanol was increased by 25% in each successive step. The samples were then dehydrated in ethanol and dried at 60 °C, in a ventilated incubator for 24 h. Iodine and bromine contents were then measured by neutron activation analysis (NAA) by the Département d'Analyse Elémentaire, Service Central d'Analyse, Centre National de la Recherche Scientifique (Vernaison, France). One analysis required 150–500 mg of algal powder depending of the total iodine in the sample, with a limit of detection (LOD) of about 10 μg g^{-1} of the dry weight.

Proton microprobe analysis and data processing

The proton microprobe, also called the nuclear microprobe, is a multielemental analytic process which simultaneously provides chemical mapping of major and trace elements at the micrometer-size level with a LOD generally in the 1–10 μg g^{-1} range. The combination of two microanalyses—particle-induced X-ray emission (PIXE) and Rutherford backscattering spectrometry (RBS)—gives access to local concentrations and, therefore, to quantitative distribution of elements. According to the nature of the samples (isolated cells, thin or thick tissue sections), these elemental distributions can be obtained at the subcellular level or at the tissue level. The principle of the proton beam microprobe and its applications in biology have been reviewed recently [32, 35].

The proton microprobe analyses were carried out at the AIFIRA platform (Applications Interdisciplinaires des Faisceaux d'Ions en Région Aquitaine) using a 3.0 MeV incident proton beam produced by a single stage Cockroft–Walton particle accelerator. PIXE and RBS analyses were performed simultaneously for determination of trace elements (Cl, K, Ca, I, Br, Fe, Zn, As) and major elements (C, N, O), respectively. The proton microbeam was focused on the sample surface to a spot of 5 or 2 μm in diameter with an estimated incoming current of 800 or 120 pA, respectively. The proton beam repeatedly scanned over the surface of the sample in a 128 × 128 pixel raster with a dwell time of 20 ms per pixel. The X-ray emission was collected using a Si(Li) energy-dispersive detector placed at 45° to the incident particles. The detection of backscattered particles was performed using a passivated implanted planar silicon detector placed at 135° to the incident beam direction.

Chemical maps were obtained from RBS and PIXE raw data using Supavisio software developed in the laboratory [36]. The chemical maps and element concentrations for Cl, K, Br, Fe, Zn and As were based on their distinctive K_α X-ray emission lines. For iodine, chemical maps were built using its L_β X-ray emission line (4.22 keV) in order to cast off the information overlapping from iodine L_α X-ray emission (3.93 keV) and calcium K_β X-ray emission (4.01 keV). Calcium chemical maps could not be displayed because of spectral interferences between calcium K_β and iodine L_α X-ray emission lines and between calcium K_α (3.69 keV) and potassium K_β lines (3.59 keV). PIXE and RBS quantitative data were processed with Gupix software [37] and SIMNRA code [38], respectively. RBS data processing provides the dried surface mass of a selected scanned area, expressed in grams per square centimeter. For each trace element detected, PIXE data processing provides its surface content expressed in micrograms per square centimeter, in the same area. Consequently, the combination of PIXE and RBS analyses allows mass normalization of the element's X-ray emission, leading to its concentrations in selected areas, expressed in micrograms per gram of dry weight, and, therefore, to its quantitative distribution. The standard error on the elemental content is determined using Gupix software [37]. For each elemental content, the standard error is calculated as the sum of the fit error, the error on the estimation of the peak area of the PIXE analysis, and the systematic error which estimates the error on the conversion of peak area to concentration.

For PIXE analyses, the LODs ranged from 2 to 220 μg g^{-1}, depending on the element detected (Table 1). The LODs of potassium and iodine were higher than those

Table 1 Proton microprobe limits of detection (*LOD*) for the elements detected in *Laminaria digitata* samples, expressed in micrograms per gram of dry weight

	K	Fe	Zn	As	Br	I	Cl	Ca
LOD	70	2	2	2	2	165	80	220

of the other elements because of the spectral interferences mentioned before. However, in spite of these high LODs, accurate quantifications were obtained since potassium and iodine contents, in the samples analyzed, were in the micrograms per gram range. Since microprobe analyses were performed on thick sections, these elemental distributions were obtained at the tissue level and refer to mean contents for several cell layers.

The whole stipe section—meristoderm, cortex and medulla—was analyzed with a probe of 5 μm diameter and over a range of 683 μm × 2,049 μm along the radial plane of the sample. An additional analysis was carried out at higher resolution, with a 2 μm-diameter probe, on the peripheral tissue of the stipe, over a range of 235 μm × 235 μm (Fig. 2). Blade sections were analyzed with the 2 μm-diameter probe, over a 500 μm × 500 μm area (Fig. 3a). The analysis time ranged from 2 to 12 h, depending on the beam size, beam current and iodine concentration in each tissue section.

SIMS microprobe and data processing

SIMS allows direct identification of elements with high sensitivity and selectivity. The SIMS microprobe can be employed to provide elemental mappings with a spatial resolution down to 50 nm. As a consequence, the SIMS microprobe has a high potential in biology to resolve the subcellular distribution of molecules of interest (trace elements, isotopes, drugs). The principle of SIMS imaging and its applications have been reviewed recently [31, 39].

SIMS analyses were performed using the Nanosims-50^{TM} ion microprobe in scanning mode (CAMECA, Genevilliers, France) at the Ion Microscopy Platform of Institut Curie (Orsay, France). The instrument is equipped with a magnetic mass spectrometer using a parallel detection system which allows the simultaneous detection of up to five species from the same microvolume. The primary ion beam was generated by a cesium source with 8-keV energy. For typical experiments, the probe was 100 nm in diameter (defined as 16–84% rise distance of the signal intensity), with an intensity of 1.5 pA. The probe scanned over the surface of the sample in a 256 × 256 pixel raster. Depending upon the analysis, the dwell time ranged from 5 to 30 ms per pixel and the width of the scanned area from 100 to 8 μm. In the present study, images of $^{12}C^{14}N^-$, $^{32}S^-$, $^{31}P^{16}O_2^{-81}$, Br^- and $^{127}I^-$ were acquired simultaneously. Bromine has two natural stable isotopes, ^{79}Br (50.5% abundance) and ^{81}Br (49.5% abundance). Since $^{79}Br^-$ is isobaric to $^{31}P^{16}O_3^-$, bromine imaging was performed by acquiring $^{81}Br^-$ in order to prevent mass interference. The magnetic field was set to detect $^{127}I^-$ on the largest-radius detector. The simultaneous detection of $^{31}P^-$ and $^{32}S^-$ was not possible because of the spacing limitation between detectors. The distribution of phosphorous was consequently obtained by the acquisition of $^{31}P^{16}O_2$. The images of $^{32}S^-$, $^{12}C^{14}N^-$ and $^{31}P^{16}O_2^-$ provide morphological and chemical features of cells. $^{12}C^{14}N^-$ and $^{32}S^-$ mostly refer to protein-like molecules. In the case of *L. digitata* samples, $^{32}S^-$ also refers to sulfated polysaccharides. $^{31}P^{16}O_2^-$ is generally used to study the distribution of phosphate-rich molecules and, consequently, to localize nuclei.

For each anion detected, the raw data are a 16 bit 256 × 256 pixel image resulting from the probe scanning over the surface of the sample. The intensity of each pixel corresponds to the direct local measurement of flux of the secondary ions. Image processing was performed using ImageJ software [40], a public-domain Java program. In what follows, SIMS elemental images are presented with a log scale.

Results

Quantitative elemental distributions in a stipe section by proton microprobe analysis

PIXE elemental maps, recorded on cryofixed stipe sections of *L. digitata* with a lateral resolution of 5 μm, indicate that the distribution of iodine has a huge, decreasing gradient of concentration from the outer cell layers to the central medullary tissues. As presented in Fig. 1a for a single stipe section, the concentration of iodine decreases from 52.8 ± 1.6 mg g^{-1} in the outer cell layers to 1.3 ± 0.2 mg g^{-1} in the cortex and 0.6 ± 0.2 mg g^{-1} in the medulla. From these data, it can be assessed that about 80% of the total iodine content is located in the meristoderm and the first cell layers of outer cortex, which correspond to about 20% of the stipe section area.

The content of bromine, the other main trace halogen, also reaches higher levels in the peripheral tissue, but its concentration gradient is less pronounced than that of iodine, leading to a homogeneous distribution through the inner cortex and the medulla. In the peripheral tissue, the concentration of bromine is lower than that of iodine, with an average of 4.2 ± 0.1 mg g^{-1} (Fig. 1b). However, in the cortex and the medulla, the bromine concentrations lie between 1.65 ± 0.04 and 1.02 ± 0.02 mg g^{-1}, which are

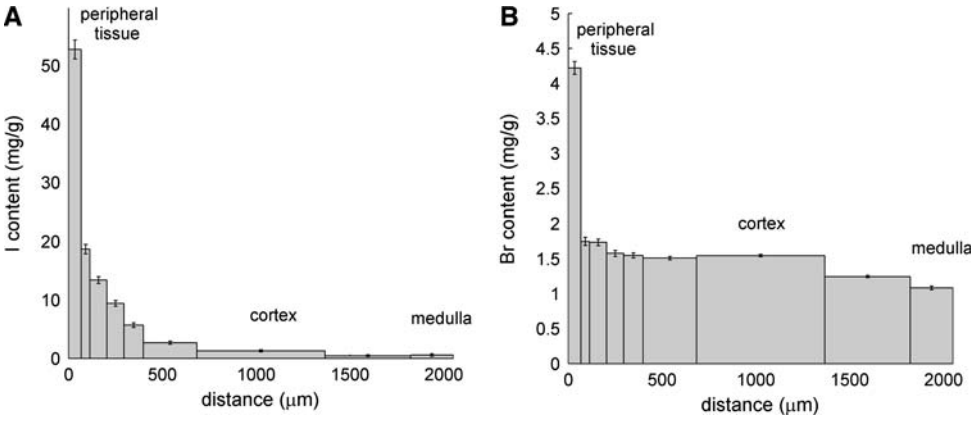

Fig. 1 Quantitative elemental distributions of iodine and bromine in a stipe section **a** Quantitative distribution profile of iodine in a *Laminaria digitata* stipe section (content in the selected area ± standard error). **b** Quantitative distribution profile of bromine in a *L. digitata* stipe section (content in the selected area ± standard error)

similar to the concentrations of iodine. The analysis carried out with a 2-μm-diameter probe reveals that the highest local concentrations of iodine and bromine are reached in the meristoderm: 191 ± 5 and 15.4 ± 0.3 mg g^{-1}, respectively. Finally, the average amounts of iodine and bromine in this stipe section are 4.2 ± 0.2 and 1.51 ± 0.02 mg g^{-1}, respectively.

The distributions of chlorine and potassium notably differ from those of iodine and bromine (Fig. 2). They are less abundant in the peripheral tissue (25 ± 1.5 and 52 ± 2.2 mg g^{-1}, respectively) than in the cortex and the medulla, in which their concentrations are relatively constant (about 109 ± 2.6 and 120 ± 2.6 mg g^{-1}, respectively). The distribution of calcium is homogeneous, with the concentration ranging from 7.6 ± 0.4 to 10.8 ± 0.6 mg g^{-1} in the cortex and the medulla. Calcium is likely to be more abundant in the meristoderm, but its content could not be properly quantified because of the spectral interferences induced by the high amount of iodine. Trace metal elements, namely, arsenic, zinc and iron, are mainly located in the peripheral tissue. Their concentrations dramatically decrease through the cortex similarly to that of iodine (data not shown). The distribution maps of carbon and nitrogen, obtained by RBS analyses, suggest that the peripheral tissue is a denser structure than the cortex and the medulla (Fig. 2).

The quantitative elemental distributions described above were similar in two other sections of stipes (data not shown).

Quantitative elemental distributions in a blade section by proton microprobe analysis

The quantitative distributions described below were similar in one further sample of blade (data not shown).

The distribution of iodine in blade sections shows a decreasing concentration gradient from the meristoderm to the medulla; however, this gradient is less pronounced than in stipe sections. As presented in Fig. 3b for a single blade section, the concentration decreases from 5.4 ± 0.6 mg g^{-1} to the LOD. In this section, the average content of iodine is about 1.7 ± 0.2 mg g^{-1}.

The bromine distribution is almost homogeneous in blade sections. As presented in Fig. 3c for a single blade section, the concentration of bromine ranges from 1.72 ± 0.07 to 0.90 ± 0.03 mg g^{-1}. In contrast to iodine, the highest levels are not found in the meristoderm but in the outer cortex. The average concentration of bromine in this blade section is 1.21 ± 0.01 mg g^{-1}, which is close to the average content measured in the previous stipe section.

As observed in stipe sections, the concentration of chlorine is lower in the meristoderm (73 ± 3 mg g^{-1}) than in the cortex and the medulla (between 136 and 177 ± 5 mg g^{-1}). However, the distribution of potassium is heterogeneous, with higher levels in the cortex, which is similar to the bromine distribution. The average concentration of potassium in the blade section is noticeably lower than in the stipe section (42 ± 1 compared with 117 ± 2.5 mg g^{-1}) (Fig. 3a). The concentration of calcium is also relatively constant in the blade section and ranges from 12.1 ± 0.6 to 14.8 ± 0.8 mg g^{-1}. As expected, trace metal elements, namely, zinc, iron and arsenic, are mainly located in the peripheral tissue (data not shown).

In conclusion, in *L. digitata*, iodine is mainly located in the peripheral tissue—the meristoderm and the first cell layers of outer cortex—in which very high local contents are measured. The highest contents of bromine are also detected in the peripheral tissue, whereas the lowest concentrations of chlorine, the other main halogen, are clearly measured in the meristoderm.

Determination of iodine and bromine content in chemically fixed and cryofixed dry tissues by NAA

The iodine content is 11.70 mg g^{-1} in a cryofixed blade sample and decreases to 0.50 mg g^{-1} in a chemically fixed

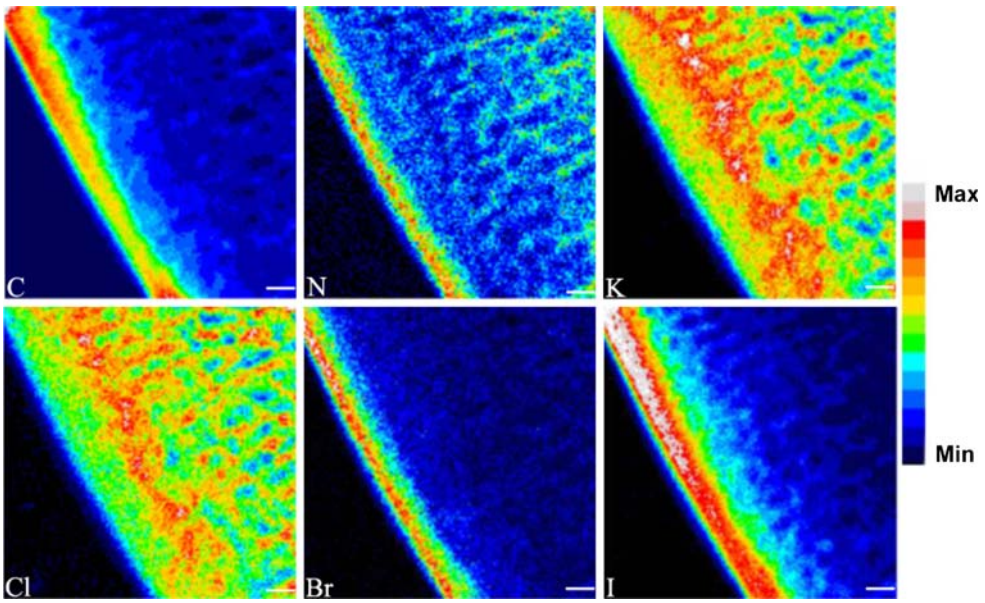

Fig. 2 Rutherford backscattering spectrometry (RBS) and particle-induced X-ray emission (PIXE) elemental maps of the meristoderm and the outer cortex in a *L. digitata* stipe section obtained with 2-μm spatial resolution. Field of view 235 μm. *Scale bar* 25 μm. Min–max bar units are arbitrary

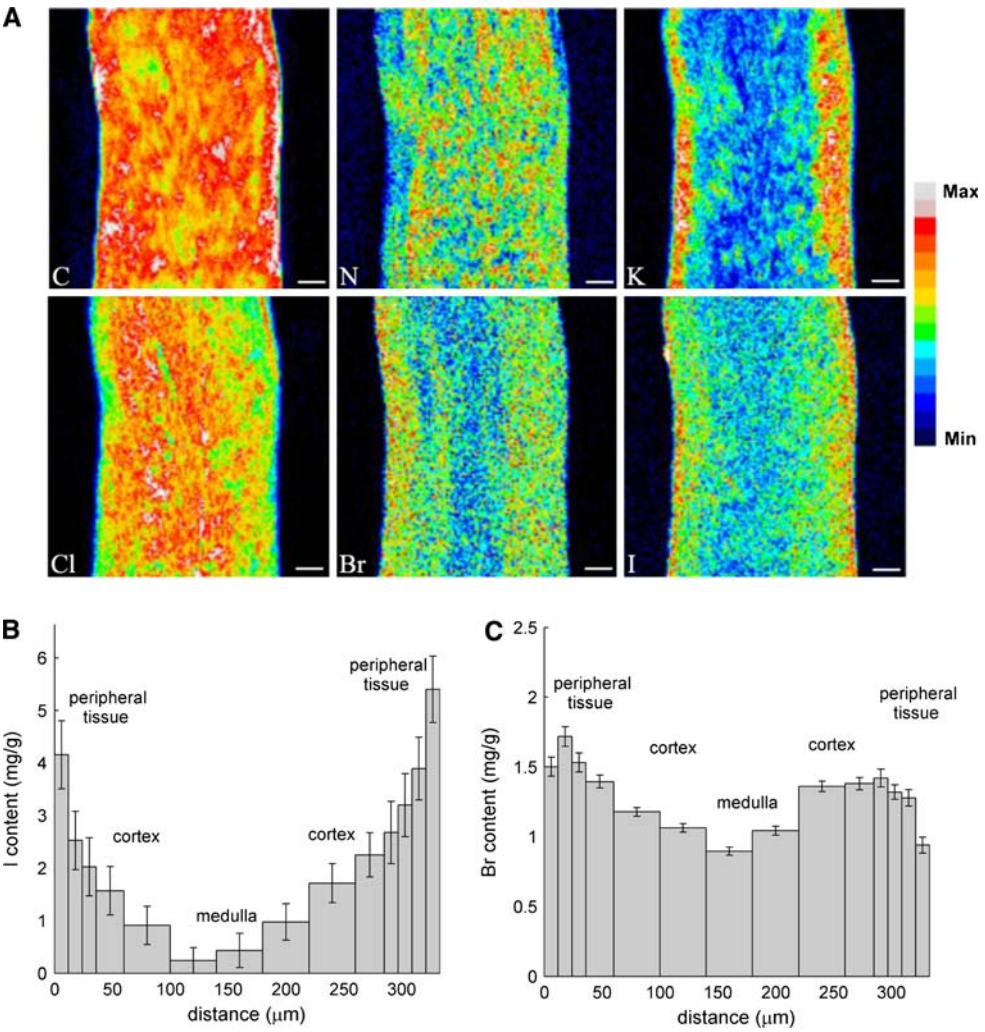

Fig. 3 Quantitative elemental distributions of iodine and bromine in a blade section. **a** RBS and PIXE elemental maps of a *L. digitata* blade section obtained with 2-μm spatial resolution. Field of view 500 μm. *Scale bar* 50 μm. Min–max bar units are arbitrary. **b** Quantitative distribution profile of iodine in a *L. digitata* blade section (content in the selected area ± standard error). **c** Quantitative distribution profile of bromine in a *L. digitata* blade section (content in the selected area ± standard error)

blade sample. In stipe from cryofixed plants, the iodine content is 19.10 mg g^{-1}, whereas in chemically fixed stipe samples it only reaches 1.14 mg g^{-1}. The bromine content of a cryofixed blade sample reaches 0.53 mg g^{-1} and decreases in a chemically fixed blade sample to 0.16 mg g^{-1}. Surprisingly, the bromine content is 0.21 mg g^{-1} in cryofixed stipe samples, whereas in chemically fixed stipe samples, it reaches 0.61 mg g^{-1}.

Subcellular distribution of iodine and bromine in chemically fixed sections by SIMS microprobe analysis

SIMS imaging was performed on chemically fixed blade and stipe sections from several sporophytes and, as mentioned earlier, gave access to the subcellular distributions of sulfur, CN, iodine and bromine. As shown in Fig. 4a, the localization of CN and sulfur provides cell structures by delimiting cell walls, cytoplasm, intercellular spaces and, even, some organelles such as plastids. The scanning of blade and stipe sections from young and old sporophytes provided similar distribution profiles for iodine as well as for bromine.

At the tissue level, iodine and bromine are mainly detected in the first cell layers, i.e., in the meristoderm and the outer cortex (Fig. 4a). In inner tissues, the signal intensity dramatically decreases. Concerning the subcellular distribution, iodine and bromine are mostly located in the apoplast i.e., in cell walls, middle lamellae and external mucilage. For both halogens, the main storage compartment is unambiguously the external mucilage i.e., the mucus layer which protects the outer meristodermic cells (Fig. 4). Intense signal spots of iodine and bromine are locally detected in extracellular spaces of the very first cell layers. By contrast, the signal intensities of iodine and bromine are very low in intracellular spaces. However, in chemically fixed sections from old sporophytes, iodine and bromine are occasionally detected in intracellular organelles which display intense signals of sulfur and CN (data not shown).

Surprisingly, bromine and iodine are not clearly colocated in the external mucilage. The scanning of this area with a field of 8 µm reveals that bromine is mainly located in the outer part of the mucilage, whereas iodine is mainly located in the inner part, close to the first meristoderm cell layer. Unlike sulfur, the signals of iodine, bromine and CN are heterogeneous. Intense spots of bromine and iodine seem to be correlated with those of CN (Fig. 4b).

Subcellular distribution of iodine and bromine in cryofixed sections

Cryofixed sections were obtained from blade of young sporophytes (less than 80 cm). The SIMS microprobe analyses were limited to the peripheral tissue which was well infiltrated in contrast to the inner cortex and the medulla. The mapping of CN and sulfur provides the delimitation of cells and the apoplast and occasionally reveals some organelles such as plastids (Fig. 5). However, the distinction of vacuoles and cytosol is not obvious. From a histological point of view, the cellular structures observed in chemically fixed and cryofixed sections are almost

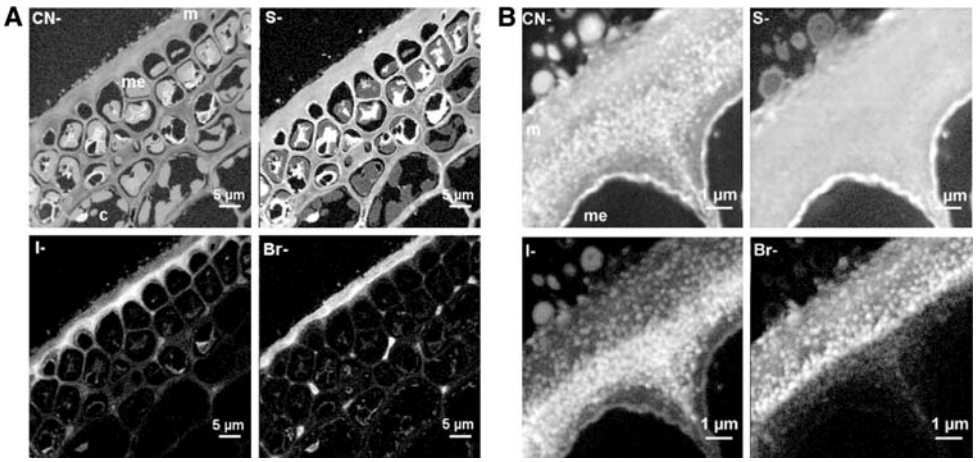

Fig. 4 Secondary negative ion images of a chemically fixed stipe section from a young *L. digitata* sporophyte. **a** In the peripheral tissue, clearly showing the apoplastic distribution of iodine and bromine. **b** In the external mucilage, which is the main storage compartment, iodine is mainly located in the inner part of the mucilage, whereas bromine is located in the upper part. The distributions of both iodine and bromine are heterogeneous. Intense iodine and bromine signals correspond with strong CN features. Each image is represented in a particular log scale in gray value levels (0–255). Field of view 50 µm (**a**) and 8 µm (**b**). Dwell time 5 ms per pixel (**a**) and 30 ms per pixel (**b**). *m* mucilage, *me* meristoderm, *c* cortex

similar; however, in the case of cryofixed sections, an additional structure is observed, just above the external mucilage. This structure shows a heterogeneous composition and presents a lot of particles with intense signal spots of CN, sulfur, bromine and iodine (Fig. 5a). These particles may refer to secretion vesicles but the image of $^{31}P^{16}O_2^-$ suggests also a bacteria film (data not shown).

Like for chemically fixed sections, SIMS imaging on cryofixed sections shows that iodine and bromine are mainly located in the apoplast, which contains approximately 60% of the total iodine and bromine signals in the area analyzed. However, in cryofixed sections, the external mucilage is not the main storage compartment of iodine and bromine. In the apoplast, the most intense signals are detected in cell walls and intercellular spaces (Fig. 5a). In these compartments, the signals of iodine and bromine are clearly correlated with strong sulfur and CN signals (Fig. 5b).

The scanning of the first cell layer, with a field of 8 μm, reveals several well-delimited intracellular structures, with very intense signals of iodine and bromine, just below the mucilage. The CN and sulfur maps and light microscopy observations do not allow their identification. These structures are not observed in chemically fixed sections, which suggests a labile content. It is noticeable that the adjacent intracellular compartment displays very weak iodine and bromine signals, which suggests a very high local concentration gradient (data not shown).

In inner cell layers, such structures are not observed. The intracellular signal of iodine is very weak and heterogeneous. From these data, the characterization of an intracellular compartment of iodine localization—such as vacuole or physode—cannot be done and may require an improvement of the dehydration and the infiltration procedures. In the case of bromine, the intracellular signal is indistinguishable from the background noise and, therefore, no intracellular compartment of storage can be identified (Fig. 5a).

Discussion

Requirements for imaging of iodine and bromine distributions in kelp tissues and cells

The use of cryofixation methods for sample preparations is crucial to preserve the iodine distribution in the algal tissues. In the case of chemical fixation, the successive aqueous and ethanol rinses resulted in a loss of labile iodine, as illustrated by NAAs. The iodine content of chemically fixed material ranges from 0.50 to 1.14 mg g^{-1}, which represents only 4–6% of the iodine content in the corresponding cryofixed tissues. These results are consistent with previous studies on iodine speciation in *L. japonica* [19] and reveal that iodine is mainly stored in a labile form. Consequently, the cryofixation procedures, described in the present study, prevented the diffusion and the leaching of labile species by the use of the freeze-drying process to dehydrate samples [31] and can be assumed to give an accurate distribution of total iodine and bromine.

Because of aqueous and ethanol rinses, the chemical fixation implied the leaching of the soluble iodine species from samples. However, a small part of these species might

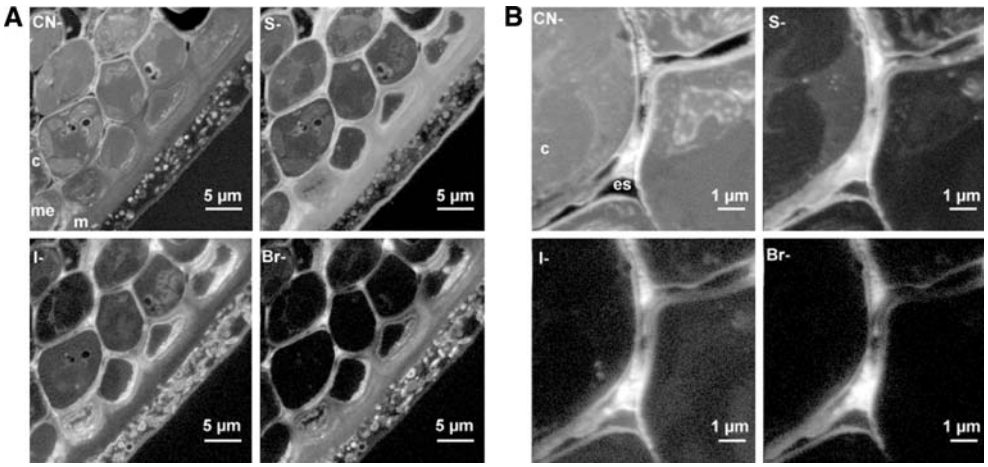

Fig. 5 Secondary negative ion images of the peripheral tissue of a cryofixed blade section from a *L. digitata* young sporophyte. **a** In the peripheral tissue, the distribution of iodine and bromine is mainly apoplastic. **b** In the intracellular space, iodine and bromine signals are clearly correlated with CN and sulfur features. Each image is represented in a particular log scale in gray value levels (0–255). Field of view 30 μm (**a**) and 8 μm (**b**). Dwell time 15 ms per pixel (**a**) and 30 ms per pixel (**b**). *m* mucilage, *me* meristoderm, *c* cortex, *es* extracellular spaces

be relocated or trapped by high-density structures. The problem is that one cannot quantify the residual proportion of these relocated species.

In the case of our study, the analyses of chemically fixed sections by the SIMS microprobe show that bromine and iodine are not colocated in the mucilage: iodine is detected in the inner part, whereas bromine is detected in the upper part of the mucilage (Fig. 4b). This kind of distribution cannot be due to the relocation of diffusive species, which would imply a homogeneous and similar distribution for both iodine and bromine species in the apoplast. In accordance with NAAs, previous speciation studies and SIMS observations, we strongly suggest that the relocated labile iodine species accounts for a very small part of the iodine content in chemically fixed sections. Consequently, the analyses of these latter sections mostly provide the distribution of strongly bound forms.

The bromine content of chemically fixed sections is similar to that of cryofixed sections. This result suggests that a significant part of bromine is strongly bound in *L. digitata* tissues or that the NAA determination of bromine content may suffer from a lack of sensitivity, as mentioned previously by Ar Gall et al. [7].

The sections obtained by the cryofixation procedure, described by Guerquin-Kern et al. [34], were suitable for the analyses of the peripheral tissue by the SIMS microprobe. However, the dehydration and the infiltration procedures of algal samples will require further improvement in order to allow fine analyses of inner tissues and intracellular structures by both the SIMS microprobe and the transmission electron microscopy.

From a technical point of view, the proton microprobe still displays limitations for subcellular elemental mappings in terms of resolution and sensitivity, so the subcellular analyses of thin sections from *L. digitata* samples could not be carried out in a reasonable acquisition time. On the other hand, the elemental absolute quantification for complex biological samples by the SIMS microprobe still remains a challenge because of the matrix effect [31, 41]. In the case of our study, the combined use of these two imaging techniques allowed us to overcome their respective limitations.

The distribution of iodine and bromine is peripheral and apoplastic

Proton microprobe analyses show that the average amounts of iodine in blade and stipe cryofixed sections from *L. digitata* are 1.7 ± 0.2 and 4.2 ± 0.2 mg g^{-1}, respectively. Blade samples were taken close to the meristematic area from algae harvested in summer, which explains their low iodine contents in comparison with spring samples analyzed by NAA [7, 23]. The average content of bromine in *L. digitata* sections is about 0.1–0.2% of dry weight, which is close to the amount determined in *L. japonica* samples [42]. The tissue distribution of iodine clearly shows a huge, decreasing gradient from the meristoderm (191 ± 5 mg g^{-1}) to the medulla (0.6 ± 0.2 mg g^{-1}) (Figs. 1a, 2). Blade sections display a similar distribution but with a less pronounced gradient (Fig. 3). Iodine is mainly stored in the meristoderm and in the outer cortex. In the case of the samples analyzed, we found that around 50 and 80% of the total iodine seems to be located in the peripheral tissue, for blade and stipe sections, respectively. Such a result confirms the previous study on *L. hyperborea* stipe sections [16] and illustrates the ability of the meristoderm to sequestrate iodine.

Similarly to iodine, the highest contents of bromine are detected in the peripheral tissue (Figs. 1b, 3c); however, the bromine concentration gradient is less pronounced than that of iodine, and their distributions within the peripheral tissue of the blade differ.

Proton microprobe analyses show that the tissue distribution of iodine is not clearly correlated with that of another element. However, it can be noticed that the meristoderm—especially that of stipe sections—has a distinctive composition, which may explain its high ability to sequestrate iodine. The meristoderm displays a denser structure, lower contents of chlorine and potassium, but higher contents of calcium and of metal trace elements (Fe, Zn, As) than the cortex and the medulla.

Unexpectedly, SIMS analyses of cryofixed sections show that bromine and iodine are mostly located in the apoplasm (Fig. 5a) and not in the cytosol or in vacuoles, as previously proposed in the literature. In the cortex, iodine and bromine are detected in cell walls and intercellular spaces. The signals of iodine and bromine in the cytoplasm of cortical cells are clearly undistinguishable from the background noise. These results clearly show that the main storage compartment of iodine and bromine is the apoplasm.

Nevertheless, very intense iodine and bromine signals are also detected in intracellular peripheral structures of meristodermic cells. These structures cannot be properly identified by photonic microscopy and SIMS imaging. However, we can assess that they do not refer to vacuoles because of their intense CN and sulfur signals, which suggests high contents of proteins and polysaccharides (data not shown). Since these structures are not observed in chemically fixed sections, their contents are likely to be easily leached. Their shape, their putative content and their intracellular localization—just below the mucilage—suggest secretion vesicles, as described by Evans and Holligan [43] in sections from the brown alga *Dictyota dichotoma*.

As described above, the chemically fixed sections allow us to study mainly the distribution of strongly bound iodine and bromine species (e.g., to macromolecules or other insoluble species). Their analyses by the SIMS microprobe clearly show that these species are located in the apoplast (Fig. 4). The external mucilage is unambiguously the main storage compartment which confirms and refines the results of Pedersen and Roomans [30]. Historical observations [44] and studies on the localization of peroxidase activities suggest that the vHPO enzymes are mainly cortical and apoplastic [45, 46]. Since these enzymes catalyze the apoplastic oxidation of halides by H_2O_2 to provide free-halogenating species [47], they may participate in the synthesis and the localization of strongly bound iodine and bromine species.

The nature of iodinated and/or brominated organic compounds is still unknown. However, according to the correlation of bromine, iodine and CN signals shown in Fig. 4b, halogenated compounds may refer to polyamides, such as proteins. This hypothesis is strengthened by old reports [18, 48] and by recent investigations using anion-exchange chromatography coupled with inductively coupled plasma mass spectrometry, which revealed the presence of monoiodotyrosine and diiodotyrosine in hydrolyzed protein fractions from brown algae samples [20]. Moreover, X-ray absorption spectroscopy (XAS) analyses on the native vanadium-dependent bromoperoxidase from the brown alga *Ascophyllum nodosum* also showed the incorporation of iodine and bromine in aromatic residues [49].

In conclusion, the analyses of cryofixed sections by proton and SIMS microprobes clearly show that the distribution of iodine and bromine is both peripheral and apoplastic. The analyses of chemically fixed sections by the SIMS microprobe reveal that the strongly bound and insoluble iodine and bromine species are also located in the apoplast. These results strongly suggest that the extracellular compartment is the main site of iodine and bromine metabolism in *L. digitata* tissues.

According to the analyses of cryofixed sections by the SIMS microprobe, bromine and iodine are located in the same compartment. This fact suggests their common participation in the halogenation processes occurring in the apoplast. It can be also proposed that Br^- competes with I^- in the mechanism of uptake, as mentioned in previous studies on the properties of vHPO [26]. However, proton microprobe quantifications show that the n(I)/n(Br) ratio in the meristoderm is 30,000 times greater than the n(I)/n(Br) ratio in seawater (about 10^4 for the whole blade and stipe sections), which illustrates the high selectivity of *L. digitata* in the accumulation of iodine species. Furthermore, the analyses of chemically fixed sections reveal that strongly bound species of iodine and bromine are not strictly colocated (Fig. 4b). This fact suggests some slight differences in their mechanism of storage.

Physiological significance of the apoplastic and peripheral distribution of iodine

Iodine is mostly accumulated in the peripheral tissue, which is continuously exposed to biotic and abiotic stresses. Its subcellular localization in the apoplasm (and perhaps in ready-to-be-released meristodermic vesicles) should allow its rapid remobilization and availability to the vHPOs for the synthesis of biocide VIOCs and I_2. Moreover, the iodine tissue distribution is correlated with the location of the oxidative burst induced by exposition of oligoguluronate blocks (which mimics an alteration of the cell wall by microorganisms) [50]. Iodine may be directly involved in the antioxidative response to protect surrounding cells, which strengthens the hypothesis that VIOCs are also the products of the scavenging of reactive oxygen species [12, 51]. Consequently, the subcellular and tissue distributions of iodine are in agreement with its putative involvement in chemical defense in *L. digitata* [8].

Nevertheless, our imaging data are partly inconsistent with the uptake mechanism proposed by Shaw [25] and refined by Küpper et al. [23], in which iodine is suggested to be stored as iodide in an intracellular compartment (Fig. 6a). Our results demonstrate that, in *L. digitata* tissues, iodine is mainly sequestrated as a very labile form in the apoplast. Besides, in cryofixed sections, the iodine signals are strongly correlated to intense signals of CN and sulfur, which suggests that protein-like molecules and/or sulfated polysaccharides are involved in the storage of iodine (Fig. 5b). Consequently, we propose that these labile iodine species are trapped by an apoplastic complex composed of polysaccharides and/or polyamides (Fig. 6b). The nature and the oxidation state of these species remain unknown and have to be determined by noninvasive in vivo experiments, such as XAS microprobe analysis. According to physiological studies which underline the involvement of an oxidative process [23, 25], it can be still supposed that vIPOs play a key role in *L. digitata*'s uptake of iodine by selectively oxidizing iodide, while bromide and chloride are far more abundant in seawater (Fig. 6b).

Conclusion

Chemical imaging of *L. digitata* stipe and blade sections by proton and SIMS microprobes shows that the peripheral tissue is the main storage compartment of iodine. Both labile and strongly bound iodine species are sequestrated in the apoplasm. This subcellular distribution is inconsistent

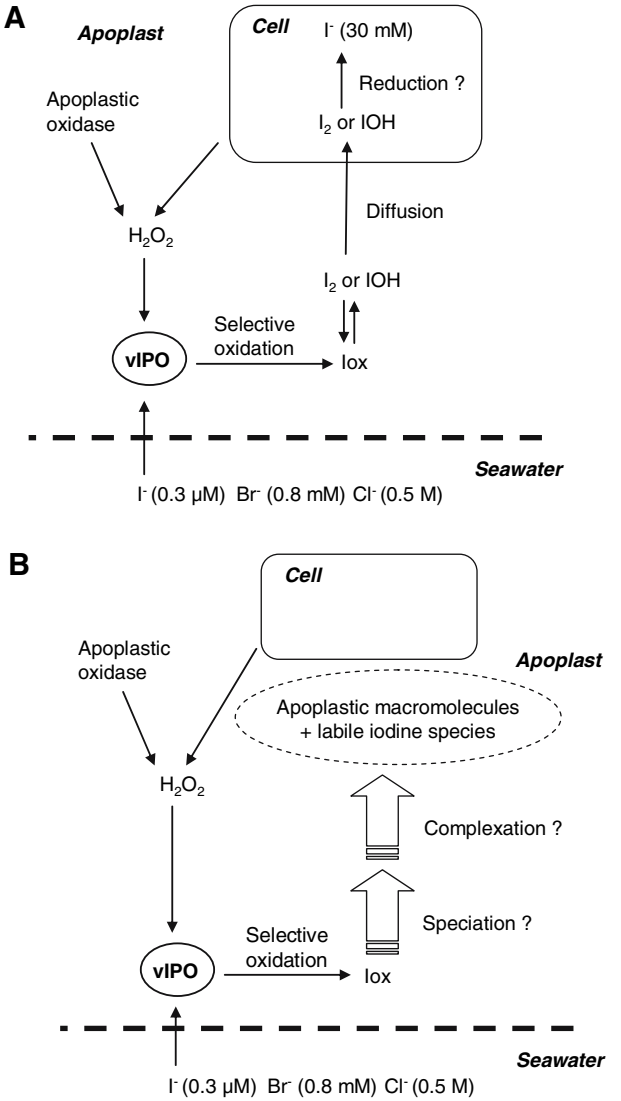

Fig. 6 **a** Mechanism of iodine uptake proposed by Küpper et al. [23]. **b** Refinement of this mechanism of iodine uptake in the light of the present imaging results. *vIPO* vanadium-dependent iodoperoxidase. (**a** Adapted from [23])

with the uptake mechanism of iodine by *L. digitata* proposed in the literature. According to our results, we suggest that iodine is mainly chelated as labile inorganic species by apoplastic macromolecules. Such a storage mechanism should provide an abundant and accessible source of inorganic iodine species, which can be easily remobilized for potential antioxidative activities and chemical defense. To the best of our knowledge, such a storage mechanism of iodine has never been described among all living systems. In mammal thyroid, iodine is accumulated within the colloid as insoluble species after the halogenation of tyroglobulin, whereas some red algae species have developed specialized gland cells with large intracellular inclusions to store small biocide iodinated molecules [52]. Consequently, the elucidation of the uptake mechanism of iodine by *L. digitata* is a real challenge and the physiological function of iodine remains to be clearly demonstrated.

From a technical point of view, the present study illustrates the sensitivity and the resolution of both proton and SIMS microprobes and demonstrates their complementarity in order to investigate the tissue and subcellular distribution of trace elements in biological samples. Therefore, the combined use of proton and SIMS microprobes provides new perspectives for physiological investigations.

Acknowledgements This study was supported by a grant from the national program Toxicologie Nucléaire Environnementale (TOXNUC-E) and by CEA and CNRS. We are also grateful to CEA and the TOXNUC-E program for PhD fellowships to E.F.V. and A.F.

References

1. Delange F (2002) Eur J Nucl Med Mol Imaging 29(Suppl 2):S404–416
2. Maberly GF, Haxton DP, van der Haar F (2003) Food Nutr Bull 24:S91–98
3. Walker SP, Wachs TD, Gardner JM, Lozoff B, Wasserman GA, Pollitt E, Carter JA (2007) Lancet 369:145–157
4. Carpenter LJ (2003) Chem Rev 103:4953–4962
5. Whitehead DC (1985) Environ Int 10:321–339
6. Fuge R, Johnson C (1986) Environ Geochem Health 8:31–54
7. Ar Gall E, Küpper FC, Kloareg B (2004) Bot Mar 47:30–37
8. Palmer CJ, Anders TL, Carpenter LJ, Küpper FC, McFiggans GB (2005) Environ Chem 2:282–290
9. O'Dowd CD, Jimenez JL, Bahreini R, Flagan RC, Seinfeld JH, Kulmala M, Pirjola L, Hoffmann T (2002) Nature 417:632–636
10. Saiz-Lopez A, Plane JMC, McFiggans G, Williams PI, Ball SM, Bitter M, Jones RL, Hongwei C, Hoffmann T (2006) Atmos Chem Phys 6:883–895
11. Laturnus F, Svensson T, Wiencke C, Oberg G (2004) Environ Sci Technol 38:6605–6609
12. Potin P, Bouarab K, Küpper F, Kloareg B (1999) Curr Opin Microbiol 2:276–283
13. Malin G, Küpper FC, Carpenter LJ, Baker A, Broadgate W, Kloareg B, Liss PS (2001) J Phycol 37(Suppl 3):32–33
14. Kolb CE (2002) Nature 417:632–636
15. Lee RE (1980) Phycology. Cambridge University Press, London, pp 481–557
16. Larsen B, Haug A (1960) Bot Mar 2:250–254
17. Tong W, Chaikoff IL (1955) J Biol Chem 215:473–484
18. Roche J, Yagi Y (1952) C R Soc Biol Paris 146:642–645
19. Hou X, Chai C, Qian Q, Yan X, Fan X (1997) Sci Total Environ 204:215–221
20. Shah M, Wuilloud RG, Kannamkumaratha SS, Caruso JA (2005) J Anal At Spectrom 20:176–182
21. Gottardi W (1999) Archiv Pharm 332:151–157
22. Hou X, Yan X, Chai C (2000) J Radioanal Nucl Chem 245:461
23. Küpper FC, Schweigert N, Ar Gall E, Legendre J-M, Vilter H, Kloareg B (1998) Planta 207:163–171
24. Kylin H (1929) Hoppe-Seylers Z Physiol Chem 186:50–84
25. Shaw TI (1959) Proc R Soc Lond Ser B150:356–371
26. Colin C, Leblanc C, Michel G, Wagner E, Leize-Wagner E, Van Dorsselaer A, Potin P (2005) J Biol Inorg Chem 10:156–166

27. Colin C, Leblanc C, Wagner E, Delage L, Leize-Wagner E, Van Dorsselaer A, Kloareg B, Potin P (2003) J Biol Chem 278:23545–23552
28. Leblanc C, Colin C, Cosse A, Delage L, La Barre S, Morin P, Fievet B, Voiseux C, Ambroise Y, Verhaeghe E, Amouroux D, Donard O, Tessier E, Potin P (2006) Biochimie 88:1773–1785
29. Klotz KH, Benz R (1993) Biophys J 65:2661–2672
30. Pedersen M, Roomans GM (1983) Bot Mar 26:113–118
31. Guerquin-Kern JL, Wu TD, Quintana C, Croisy A (2005) Biochim Biophys Acta 1724:228–238
32. Lobinski R, Moulin C, Ortega R (2006) Biochimie 88:1591–1604
33. Ortega R, Moretto P, Fajac A, Benard J, Llabador Y, Simonoff M (1996) Cell Mol Biol (Noisy-le-Grand) 42:77–88
34. Guerquin-Kern JL, Hillion F, Madelmont JC, Labarre P, Papon J, Croisy A (2004) Biomed Eng Online 3:10
35. Llabador Y, Moretto P (1998) Applications of nuclear microprobes in the life sciences: an efficient analytical technique for research in biology and medicine. World Scientific, Singapore
36. Barbotteau Y (2004) http://biopixe.free.fr/SupaVISIO/news.htm
37. Campbell JL, Hopman TL, Maxwell JA, Nejedly Z (2000) Nucl Instrum Methods Phys Res B 170:193–204
38. Mayer M (1997) SIMNRA user's guide. Max-Planck-Institut für Plasmaphysik, Garching
39. Clerc J, Fourre C, Fragu P (1997) Cell Biol Int 21:619–633
40. Rasband WS (1997–2007) ImageJ. http://rsb.info.nih.gov/ij/
41. Quintana C, Wu TD, Delatour B, Dhenain M, Guerquin-Kern JL, Croisy A (2007) Microsc Res Tech 70:281–295
42. Saenko GN, Kravtsova YY, Ivanenko VV, Sheludko SI (1978) Mar Biol 47:243–250
43. Evans LV, Holligan MS (1972) New Phytol 71:1161–1172
44. Dangeard P (1928) C R Acad Sci 186:892
45. Colin C (2004) PhD report, Ecole doctorale sciences de l'environnement d'Ile-de-France, Université Paris VI, Paris
46. Almeida M, Filipe S, Humanes M, Maia MF, Melo R, Severino N, da Silva JA, Frausto da Silva JJ, Wever R (2001) Phytochemistry 57:633–642
47. Carter-Franklin JN, Butler A (2004) J Am Chem Soc 126:15060–15066
48. Scott R (1954) Nature 173:1098–1099
49. Feiters MC, Kupper FC, Meyer-Klaucke W (2005) J Synchrotron Radiat 12:85–93
50. Küpper FC, Kloareg B, Guern J, Potin P (2001) Plant Physiol 125:278–291
51. Pedersen M, Collen J, Abrahamsson K, Ekdahl A (1996) Sci Mar 60:257–263
52. Paul NA, Cole L, de Nys R, Steinberg PD (2006) J Phycol 42:637–645